533308

Creep and Toughness of Cryomilled NiAl Containing Cr

J. Daniel Whittenberger, Beverly Aikin, Jon Salem
NASA-Glenn Research Center
Cleveland, OH 44135

ABSTRACT

NiAl-AlN + Cr composites were produced by blending cryomilled NiAl powder with ~ 10 vol % Cr flakes. In comparison to the as-consolidated matrices, hot isostatically pressed Cr-modified materials did not demonstrate any significant improvement in toughness. Hot extruded NiAl-AlN+10.5Cr, however, possessed a toughness twice that determine for the base NiAl-AlN alloy. Measurement of the 1200 to 1400 K plastic flow properties revealed that the strength of the composites was completely controlled by the properties of the NiAl-AlN matrices. This behavior could be successfully modeled by the Rule-of-Mixtures, where load is shed from the weak Cr to the strong matrix.

Creep and Toughness of Cryomilled NiAl Containing Cr

J. Daniel Whittenberger, Beverly Aikin, Jon Salem

INTRODUCTION

As a replacement for Ni/Co-based superalloys in air breathing gas turbine engines, materials based on the B2 intermetallic NiAl offer several superior characteristics [1-3]. These include a melting point on the order of 1900 K, a density of about 6 Mg/m^3 and a thermal conductivity as high as 100 W/mK; such properties compare very favorably to superalloys that melt at ~ 1600 K, weigh about 8.5 Mg/m^3 and possess thermal conductivities of 10 to 20 W/mK. Additionally the high Al content in NiAl directly leads to the formation of a long life, protective Al_2O_3 scale; whereas extended use of superalloys in a high temperature, oxygen rich atmosphere requires a protective coating that is, at least, partially composed of NiAl.

As opposed to the above advantages, the mechanical properties of NiAl are deficient in comparison to those of superalloys. In particular the elevated temperature creep strength and room temperature toughness of binary NiAl are very low. For example, the stress to produce a deformation rate of 10^{-7} s^{-1} at 1300 K is about 15 MPa for polycrystalline [4] and [001] oriented single crystalline [5,6] NiAl as opposed to 200 MPa for the single crystal Ni-based superalloy NASAIR 100 [7]. Furthermore, the toughness of polycrystalline and single crystalline NiAl is on the order of 5 to 8 MPa÷m which is about a factor of ten less than the 55 MPa÷m reported for single crystal NASAIR 100 [8].

Over the past ten years a number of different techniques have been identified to strengthen NiAl for elevated temperature use. For example Darolia and Walston [9] have demonstrated that small alloying additions in NiAl single crystals can dramatically improve the creep strength: i.e. a stress of about 100

MPa is required to produce a deformation rate of 10^{-7} s^{-1} at 1300 K in [001] oriented NiAl-1Hf[1] crystals [10]. In addition, mechanical alloying to produce dispersion strengthened NiAl[11-13] and high intensity milling of NiAl powder in liquid nitrogen {the cryomilling process} [14] have been identified as methods to hardening NiAl via powder metallurgy processing. As such, the 1300 K - 10^{-7} s^{-1} creep strength for an $Y_3Al_5O_{12}$ dispersion strengthened NiAl is about 60 MPa [11,12] while an AlN dispersion strengthened NiAl [13] or a cryomilled NiAl [14] can require stresses greater than 100 MPa for the same deformation conditions.

Although single crystal and polycrystalline technologies have significantly increased the strength of NiAl, they have not been able to positively affect the toughness [8]. To date only directional solidification (DS) of NiAl-based eutectic systems [15] has shown promise for simultaneous improvement of both the elevated temperature creep resistance and room temperature toughness, where proper DS'ing produces a NiAl matrix containing very small diameter fibers or very thin lamella that are strong at elevated temperature and are capable of ductile phase toughening at low temperatures. For example directionally solidified NiAl-31Cr-6Mo with < 1 μm thick (Cr,Mo) lamella possesses combined properties of a 125 MPa creep strength at 1300 K - 10^{-7} s^{-1} and a 20+ MPa÷m room temperature toughness [15]. One of the major difficulties with directional solidification, however, is the limitation to specific compositions which are dictated by the relevant equilibrium phase diagrams. Even small deviations from the eutectic composition during directional solidification can lead to dendrites or other coarse microstructural features that can adversely affect the mechanical properties.

The strict compositional limitation imposed by the eutectic reaction during directional solidification can be avoided through use of solid state powder blending techniques to produce puesdo-eutectic mixtures which lie within the solid state two phase equilibrium regime (for example: binary NiAl powder could be combined with elemental Cr powder to yield overall compositions of NiAl + 10 to 80 at % Cr [16]).

[1]All compositions are reported in atomic % unless noted.

While such blends are thermodynamically stable, this technique has not been successful because it is extremely difficult to reproduce the fine scale second phase microstructure necessary for high temperature strength. With the advent of strong powder metallurgy NiAl materials, however, it should be possible to eliminate or reduce this size restriction as strengthening can now be supplied by the matrix while the ductile second phase can provide toughness. This latter concept has been confirmed by blending ODS NiAl powder with 25 vol. % Mo which yielded fracture toughnesses ranging from 8 to 12 MPa÷m compared to ~4 MPa÷m for the base ODS NiAl alloy [11,17].

Even though the powder metallurgy concept of mixing a strong matrix with a ductile second phase is logical, only one recent study which involved measurement of both creep and toughness properties has been reported in the literature [18]. In this work Lane, et al. found that powder metallurgy processed pure alumina and Al_2O_3 reinforced with 20 vol % Nb exhibited similar power law creep stress exponents at 1473 K, but the deformation resistance of the composite was nearly an order of magnitude less than that of un-reinforced alumina. On the other hand, the fracture toughness of Al_2O_3 + Nb was ~14 MPa÷m compared to about 4.5 MPa÷m for alumina. Thus the observed composite behavior of a somewhat degraded creep strength with improved toughness was in agreement with general expectations.

The current study was initiated to measure both the room temperature toughness and elevated plastic flow properties of powder metallurgy puesdo-eutectic mixtures of Cr with strong cryomilled NiAl. Three pairs of alloys with and without Cr were prepared by blending melt spun Cr flakes with cryomilled NiAl powder containing either 7.5 or 12.5 vol % AlN and then densifing by hot isostatic pressing or hot extrusion. In addition to toughness measurements and 1200 to 1400 K deformation experiments, room temperature flexural bend strengths and elastic moduli were determined, and the alloys were characterized by standard metallurgical techniques.

EXPERIMENTAL TECHNIQUES

The cryomilling process as applied to NiAl has been thoroughly discussed in [14,19]. In summary cryomilling was undertaken in a Union Process Model 01-HD attritor enclosed in a slightly positive nitrogen pressure environmental chamber. The attritor vessel was filled in air with 500 g of prealloyed aluminide powder and ~2500 g of hardened steel grinding balls, loaded in the attritor and cooled by flowing of liquid nitrogen through the attritor vessel jacket. Milling was initiated once vessel contents were sufficiently cooled to submerge them in liquid nitrogen to create a slurry. During operation liquid nitrogen was constantly passed through the cooling jacket, while intermittent injections of nitrogen were made into the vessel to maintain a constant slurry level height. Two different AlN levels in NiAl were produce by milling prealloyed -325 mesh Ni~33.6 wt.% Al powder for 6 h or 9 h.

Once cryomilling was completed, the powders were allowed to warm to room temperature under a nitrogen cover gas and then separated from the grinding media. All subsequent powder handling was then accomplished in laboratory air. In order to produce sufficient powder for measurement of the matrix and composite properties, multiple attritor runs were undertaken using the same processing conditions, and the resultant powders blended together. An approximately 2 kg lot of the lower AlN content powder and a 1 kg lot of the higher AlN content powder were then separately mixed with ~10 vol. % Cr in the form of small melt spun flakes. Sufficient amounts of the lower AlN content powder and its Cr-modified version were available for densification by both Hot Isostatic Pressing (HIP) and hot extrusion. The powders were first vacuum canned in steel and then either HIP'ed at 1495 K -138 MPa - 6 h or hot extruded at 1505 K with an 8:1 reduction ration. The higher AlN content materials were also vacuum canned in steel; however they were only consolidated by HIP.

Mechanical property test specimens were prepared from the densified materials by electrodischarge machining (edm) and grinding techniques. Sample geometries included 50 mm x 6 mm x 3 mm bars for room temperature bend measurements, ASTM standard chevron notched four point bend bars (50 mm x 6 mm x 3 mm) for fracture toughness studies[20], and 10 mm tall by 5 mm diameter right cylinders for compression testing. While sample orientation was not characterized for the HIP materials, the long axis of the specimens taken from the two extruded rods was parallel to the hot extrusion direction. The major surfaces of all samples were ground to remove the recast edm surface damaged layer.

Room temperature bend testing was undertaken under four point conditions utilizing a fixture with a 40 mm span for support and a 20 mm span for loading. Bending of the 3 mm thick specimens took place under a constant velocity of 0.021 mm/s in a universal testing machine with deformation being monitored by strain gages bonded to the tensile side of the test bars. The load results were converted into outer fiber tensile stress values using the standard linear elastic bend equation which were then combined with the outer fiber tensile strain data from the strain gage to define the stress - strain curve. The elastic modulus was calculated from the linear portion of each diagram, while the yield stress was defined by the initial deviation from linearity and ultimate tensile strength was taken to be the fracture stress. The elastic moduli were also measured by applying the impulse excitation technique [21] to beam specimens.

Fracture toughness of the alloys at room temperature was measured in four-point bending by using the Single-Edge-Precracked-Beam technique in accordance with ASTM C1421 [20]. The test specimens were loaded at a stroke rate of 0.0033 mm/s with 20 and 40 mm inner and outer spans. The specimen stability was monitored by a strain gage placed on the compressive face of the specimen [22]. Prior to testing all specimens were heat treated in air for 1 h at 973 K to delineate the precrack.

The 1200 - 1400 K slow plastic deformation properties in air were determined by compressing samples between SiC push bars under constant velocity conditions in an universal testing machine and under constant load creep conditions in lever arm creep frames. The autographically recorded load - time charts from the universal test machine operating at speeds ranging from 2.1×10^{-3} to 2.1×10^{-6} mm/s were converted to true compressive stresses, strains, and strain rates via the offset method and the assumptions that volume is conserved and all plastic deformation occurred in the specimen. Creep deformation under constant load conditions was determined as a function of time by measuring the relative positions of ceramic push bars applying the load to the specimen. After normalizing the contraction - time results with respect to the final specimen length, the data were converted into true stresses and strains by assuming volume conservation. While most test samples were tested under a single load, a few creep specimens were subjected to multiple engineering stress conditions.

Light optical metallography and scanning electron microscopy (SEM) techniques were utilized to examine the microstructure of as consolidated alloys and selected samples after testing. Chemical analysis was undertaken on the densified materials to determine the matrix composition and volume fraction of second phases. Concentrations of metallic elements (Ni, Al, Cr, etc.) were determined by an inductively coupled plasma (ICP) technique, while the amounts of nitrogen and oxygen were measured by an inert gas fusion method.

RESULTS

Composition

The method of consolidation, Al content of the NiAl matrix as well as the volume fractions of ceramic phases from cryomilling (AlN and Al_2O_3) and the intentional Cr additions are presented in Table 1 for each alloy in this study. These values were estimated utilizing the following assumptions:

1. The solubility of N, O and Cr in NiAl is zero
2. All nitrogen forms AlN with a density of 3.26 Mg/m^3;
3. Oxygen forms Al_2O_3 with a density of 3.965 Mg/m^3;

4. Cr has a density of 7.19 Mg/m^3,
5. The density (ρ) of NiAl [23] in Mg/m^3 is given as a function of at. % Al (X) by

$$\rho = 1.415 + 0.267X - 0.00358X^2 \quad (1)$$

Table 1 indicates that (1) all six alloys had matrix Al contents near stoichiometry, (2) two levels of AlN were produced, and (3) Cr loadings of about 10 vol. % were achieved. The four lower AlN content alloys L24/L25 and 87/86, which all derived from the same batch of cryomilled powder, possess comparable chemistries in both the Cr-free versions (L24 and 87) and the Cr-modified forms (L25 and 87). Additionally, as a result of a longer attritor run and a slightly higher Al content in the initial prealloyed NiAl powder, the matrix Al level of 91/90 is nearly the same as those of the other four alloys even though >60 % more AlN was formed.

Microstructure

Typical examples of the unetched microstructures found in the densified Cr-modified alloys are presented in Figs.1 and 2. In the case of the extruded bar, the low magnification photomicrographs of the cross section (Fig. 1(a)) and longitudinal section (Fig. 1(b)) illustrate the distribution and morphology of the Cr flakes within the cyromilled NiAl matrix. In particular Fig. 1(a) demonstrates that the distribution of Cr is not uniform and a wide variety of flake-like cross sections exist, while Fig. 1(b) shows that the flakes are strung out in the extrusion direction. At higher magnifications it can be seen that Cr is tightly bonded to the matrix (Figs 1(c,d)), where the NiAl-AlN matrix possesses a cigar like microstructure that is small in cross section (Fig. 1(c) and elongated along the extrusion axis (Fig. 1(d)). Photomicrographs of HIP'ed materials are presented in Fig. 2, where part (a) again illustrates the wide range of Cr shapes and their distribution. Fig. 2(b) shows the good Cr to matrix bonding and the core and mantle microstructure of cryomilled NiAl, where the medium gray circular regions are the AlN-free NiAl cores.

Occasionally ceramic particles were observed in the Cr-modified alloys, as is illustrated in Fig. 2(c) for a HIP'ed alloy; such particles were also found in the extruded material containing Cr. The large ceramic second phases were generally not well bonded to the matrix and, at least in this case, promoted cracking in

the matrix. Also, particularly in the case of the HIP'ed alloys, regions of secondary precipitation along grain boundaries could be found in the vicinity of the Cr flakes (Fig 2(d)); presumably these are Cr precipitates which formed during cooling after the 1495 K consolidation exposure.

While the microstructure of the extruded materials (Fig. 1) exhibited a dependence on direction; examination of specimens taken 90° apart did not reveal any directionality in the HIP'ed alloys. Additionally the microstructure of the densified NiAl-AlN matrix alone alloys appeared to be exactly the same as the matrices in Figs. 1 and 2 away from the Cr flakes; furthermore neither ceramic particles nor small Cr precipitates were found in the consolidated matrix alloys without Cr.

Room Temperature Mechanical Properties

All six alloys were subjected to elastic modulus measurements and 4 point bend testing at room temperature; three alloys were also successfully tested for toughness to determine if the Cr flake additions improved this property. These results are given in Table 2. The reported dynamic and bend moduli, as well as, the bend yield strength and tensile fracture strength values are averages from at least duplicate measurements except for the base-line high AlN content alloy {91, Table 1}, where only a single experiment was undertaken. The toughness data are averages from a minimum of triplicate testing.

With one exception the moduli measured by the dynamic technique are 10 to 15 GPa greater than those estimated by bending (Table 2). Additionally there is no consistency between the measured moduli of the base alloys and their Cr-modifications with examples of greater than {alloys L24/L25}, approximately equal {alloys 87/86} and less than {alloys 91/90} being present. In terms of the bend strength properties (Table 2), the Cr-modified alloys have both lower yields and tensile fracture strengths than their base compositions. The decrease in fracture strength is particularly dramatic in the HIP'ed materials, where a factor of three difference exists.

Fracture toughness samples were machined from all six materials; however only four alloys could be successfully precracked. In the other two cases, the attempts to precrack resulted in cracks which were unsuitable for further testing. Although only limited toughness testing was undertaken, the data for all three HIP'ed materials {86, 87 and 90} in Table 2 are about the same which indicates that ~10 volume percent additions of Cr flakes to cryomilled NiAl does not significantly improve this property after this method of densification. On the other hand, the toughness for hot extruded NiAl-6.5AlN+10.5Cr {L25} shows almost a factor of two improvement over its HIP'ed counterpart {86} and is more than twice the toughness demonstrated by the HIP'ed base NiAl-7.4AlN composition {87}. It should be noted that scatter observed during toughness testing of L25 was much larger than that seen in the other three alloys, where values for the hot extruded Cr-modified alloy ranged from 9.3 to 13.9 MPa÷m, hence its greater standard deviation in Table 2.

Elevated Temperature Plastic Flow Properties

Examples of the plastic stress - strain curves determined under constant velocity conditions are illustrated in Fig. 3 for the two higher AlN content alloys {91/90, Table 1}. These graphs are typical for all six materials compressed between 1200 and 1400 K, where a small amount of strain hardening was followed by steady state flow or slight work softening. Additionally the strength of each alloy decreased with decreasing imposed strain rate, and the strength of the unmodified alloys (Fig. 3(a)) was greater than their Cr-modified versions (Fig. 3(b)) at each deformation rate.

Typical creep curves for two base-line alloys and their Cr-modified forms {91/90 and L24/L25, Table 1} are illustrated in Fig. 4, where each specimen was subjected to several engineering stresses at 1300 K. Irrespective of the material or temperature, normal creep curves were developed for each set of test conditions. Also, as is shown for the HIP'ed higher AlN (Fig. 4(a)) and hot extruded lower AlN content

(Fig. 4(b)) materials, creep testing again revealed that the Cr-modified alloys were less creep resistant than their unmodified base compositions.

True compressive flow stress - strain rate - temperature results for all six alloys are presented in Fig. 5. In this figure the flow stresses evaluated from constant velocity testing {open symbols} are represented by the stress at 3 % strain from the stress - strain curves (Fig. 3), while the flow stresses from creep testing {solid symbols} are the average stresses calculated over each steady state regimes (Fig. 4). Only constant velocity testing was undertaken for the HIP'ed lower AlN content alloys (Figs. 5(a,b)); however both test methods were used for the hot extruded lower AlN (Fig. 5(c,d)) and HIP'ed higher AlN content materials (Figs. 5(e,f)). This latter group of flow stress - strain rate - temperature data (Figs. 5(c-f)) indicate that both constant velocity and creep testing yielded consistent results.

Although a temperature compensated power law could describe some of the time dependent plastic flow data shown in Fig. 5, it was found that all the flow stress (σ) - strain rate ($\dot{\varepsilon}$) - temperature (T) results could be represented by a temperature compensated exponential equation

$$\dot{\varepsilon} = A \exp(C\sigma)\exp(-Q/(RT)), \qquad (2)$$

where A is a constant, C is the stress constant, Q is the activation energy for deformation and R is the universal gas constant. Each set of data were fitted to eqn (2) by linear regression techniques, and the resultant values for A, C, Q and the standard deviations for the stress constant (δ_C) and activation energy (δ_Q) as well as the coefficients of determination (R_d^2) are give in Table 3(a). Additionally the results of the regression analyses are portrayed by the curves in Fig. 5. Based on visual inspection and the coefficients of determination (Table 3(a)), eqn (2) describes the experimental data for each material well. Additionally, comparison of C and Q for each base alloy and its Cr-modification {87/86, L24/L25 and 91/90, respectively, Table 3} indicates that these deformation parameters have essentially the same values for each pair. While the stress constant for the HIP'ed lower AlN content alloys {87/86, Table 3(a)} is about

33 % greater than those measured for either the hot extruded lower AlN content or HIP'ed higher AlN content materials {L24/L25 and 91/90, respectively, Table 3(a)}, the activation energy for deformation for all six materials appears to be about ~500 kJ/mol.

DISCUSSION

As-consolidated materials

With one exception the microstructure of the Cr-free and Cr-containing alloys fulfilled expectations: in particular {1} the appearance of the cryomilled matrix microstructure (Figs. 1(c,d) and 2(b)) was in agreement with previous studies of extruded and HIP cryomilled NiAl [14]; {2} the powder blending/densification techniques in combination with a low volume fraction of relatively large, flake-like particles did not produce a particularly uniform distribution of Cr in the matrix (Figs. 1(a,b) and 2(a)); {3}an apparent good metallurgical bond between the matrix and Cr flakes (Figs. 1(c,d) and 2(b,d)) was established; and {4} small precipitates, probably Cr, were found in the vicinity of Cr flakes (Fig. 2(d)). The excellent contact between Cr and NiAl is a direct consequence of the eutectic formed between NiAl and Cr [16,24], and this result agrees with the strong metallurgical bond found between ODS NiAl and Mo [11]. The belief that the small precipitates near Cr flakes are, indeed, chromium is due to the high Cr solubility in NiAl at the consolidation temperature (approaching 10 % at 1500 K) which decreases rapidly on cooling [16,25].

The unexpected microstructural feature was the occasional large ceramic particle in the Cr-modified alloys (Fig. 2(c)), where such chunks are probably pieces of the crucible from the melt spinning step to produce Cr flakes. While the large particles would have very little effect on elevated temperature compressive strength behavior, they are likely to be the source of premature failure at low temperatures, particularly if they induce cracking in the matrix as demonstrated in Fig. 2(c).

Because of the inability to precisely determine the Al content of NiAl closer than about ± 0.5 at % [26], the Al level is probably identical in the two unmodified {87 and L24, Table 1} versions of the low AlN content alloys. Likewise, the composition of NiAl matrix must be essentially the same in the two Cr-modified low AlN content alloys {86 and L25, Table 1}. With the addition of about 10 volume % Cr to the matrix, the overall AlN and Al_2O_3 contents in the three Cr- modified alloys should decrease approximately 10 % compared to the matrices alone. Clearly the AlN results in Table 1 are in agreement with this contention; while the alumina levels are not, possibly due to their low initial values in the as-cryomilled powders and some oxygen contamination from the Cr.

Room Temperature Behavior

Sufficient information exists in Table 1 and the literature to allow Rule of Mixture estimations of the elastic moduli of the HIP'ed alloys. Since the modulus of NiAl is not very sensitive to composition [3], a Young's modulus of ~188 GPa, which was measured at room temperature on prealloyed Ni-50.6Al powders consolidated by hot pressing [3], is an appropriate value for all the HIP matrices. Combination of this value in the Rule-of-Mixtures along with elastic moduli of 308 GPa for AlN [27] and 253 GPa for Cr [28] and the appropriate volume fraction data (Table 1) yields the predicted moduli in Table 1. These Rule-of-Mixtures predictions are in good agreement with those determined by the dynamic method and, thus, higher then those determined by bend testing.

Similar Rule-of-Mixtures calculations could have been undertaken for the two hot extruded alloys {L24/L25}; however previous work [3] has shown that the modulus of hot extruded NiAl powder is much higher than HIP'ed powder due to a preferred crystallographic orientation: for example the modulus of hot extruded Ni-50.6Al is ~ 243 GPa [3]. Neither the dynamic nor bend elastic moduli results for L24/L25 (Table 2) support the idea that the extruded alloys were oriented parallel to a high modulus direction; if anything, based on the data in Table 2, the preferred orientation of L24/L25 would have to be along an elastically compliant direction. Recently, Wolfenden, et al [29] have measured the room

temperature dynamic Young's moduli of cryomilled, HIP'ed NiAl-5 vol % AlN and cryomilled, hot extruded NiAl-10 vol % AlN and obtained values of 292 and 266 GPa respectively. These results are much greater than those obtained in the current study (Table 2), and they are much greater than any Rule-of-Mixture prediction based on values for NiAl and AlN.

The room temperature tensile properties of the unmodified and Cr-modified cyromilled NiAl alloys (Table 2) estimated by bend testing indicate that these materials are lacking in low temperature strength. Even the strongest of the unmodified alloys {87} had a yield strength which is a factor of ~7 lower than that determined in NiAl-8.4 vol % AlN by compression [30]. Compared to the base compositions, all three Cr-modified alloys suffered a loss of yield strength and a dramatic decrease in the estimated tensile fracture strengths. Part of this degradation could be due to ceramic particles accompanying the Cr-flake additions (Fig. 2(c)) or the Cr flakes, themselves, acting as a crack. If the latter were true, one could expect a difference in tensile strength as the size of Cr was changed. Since extrusion refines the flake thickness compared to HIP, the fracture stress of the extruded material should exceed that measured for the HIP version which agrees with the results determined for alloys L25 and 86 in Table 2.

Previous measurements indicated that the room temperature toughnesses of NiAl and HIP'ed or extruded cryomilled NiAl containing from 5 to 30 vol % AlN ranged from 5 to 6 MPa$\sqrt{m}$ [30]. As the 4.6 MPa$\sqrt{m}$ toughness measured for the unmodified alloy 87 (Table 2) is in essential agreement with this work, the results obtained for the Cr-modified alloys should also be valid. While the toughness values for the two HIP'ed alloys are not significantly greater than that measured for the unmodified NiAl-AlN, the data for hot extruded NiAl-6.4AlN+10.5Cr {L25} strongly suggest that meaningful second phase toughening is possible even with a relatively low volume fraction of Cr. The increased toughness of hot extruded alloy L25 in comparison to the HIP alloys must be due to a change in the microstructure, where extrusion elongates the Cr flakes thus making the present composite more like a directionally solidified NiAl-Cr eutectic. Furthermore, based on a 20 MPa$\sqrt{m}$ toughness for directionally solidified NiAl-Cr

containing ~34 vol % of submicron thick Cr fibers/lamella [31], additional improvement in the toughness of hot extruded NiAl-AlN+Cr should be possible by increasing the Cr content.

Although the combination of Cr and hot extrusion did result in a significant improvement in room temperature toughness (Table 2), the scatter in the measured values is bothersome. Hence further testing of L25 is needed and has been planned.

Creep Properties

The nearly alike stress constants and activation energies for deformation for each pair of base and Cr-modified alloys in Table 3(a) strongly suggest that elevated temperature plastic flow properties could be described a single temperature dependent exponential equation with different A coefficients for each material. The results of such linear regression analyses are presented as solid (base alloy) and dashed lines (Cr-modified alloy) in Fig. 6 with the appropriate parameters and statistical characteristics being given in Table 3(b). Comparison of Figs. 5 and 6 and the regression coefficients in Table 3 indicate that deformation for each set of base/Cr-modified alloys can be described with a unique stress constant and activation energy.

The ability to use eqn (2) with the simplified parameters in Table 3(b) to describe the elevated temperature plastic flow properties of cryomilled NiAl with and without Cr allows several comparisons to be easily made. For example a strength difference between hot extruded (L24) and HIP'ed (87) forms of NiAl-7.4AlN can be directly visualized from the mathematical descriptions given in Table 3(b), where both have similar A values {1.88×10^9 and 1.45×10^9} and activation energies {-481.4 and -474.7} but different C's {0.0805 versus 0.0605}. The lower C parameter for hot extruded NiAl-7.4AlN compared to the HIP'ed version indicates that the hot extruded alloy would creep at a slower rate for any given combination of stress and temperature; thus the hot extruded L24 is stronger. Furthermore, exactly the

same argument can be made for the hot extruded (L25) and HIP'ed (86) NiAl-6.5AlN+10.3Cr materials. By visually contrasting the data in Figs. 5(a) and 5(c) for the HIP'ed and hot extruded versions of NiAl-7.4AlN and the results in 5(b) and 5(d) for the HIP'ed and hot extruded versions of NiAl-6.5AlN+10.3Cr, the strength differences can be somewhat quantified, where the hot extruded versions are 10 to 30 % stronger that the HIP'ed materials.

The simplified parameters in Table 3(b) can be also used to quantify the difference in strength between each base NiAl-AlN alloy and its Cr-modified form. For any strain rate

$$\dot{\varepsilon} = A_{Base} \exp(C\sigma_{Base})\exp(-Q/(RT)) = A_{Comp} \exp(C\sigma_{Comp})\exp(-Q/(RT)), \qquad (3)$$

where A_{base}, A_{comp} and σ_{Base}, σ_{Comp} are the creep deformation constants and stresses for the base alloy and its Cr-modified form. This equation can then be rearranged and reduced, as C and Q are identical for both forms, to give the strength difference which is independent of the strain rate or temperature,

$$\sigma_{Base} - \sigma_{Comp} = \ln(A_{base}/A_{comp})/C \qquad (4)$$

Thus the strength difference between HIP'ed NiAl-7.4AlN {alloy 87} and NiAl-6.5AlN+10.2Cr {alloy 86} is estimated to be 15.2 MPa, between hot extruded L24 (NiAl-7.3AlN) and L25 (NiAl-6.5AlN+10.5Cr) it should be 29.8 MPa, while a 39.2 MPa difference would be found between HIP'ed NiAl-12.4AlN {alloy 91} and NiAl-11.4AlN+11.1Cr {alloy 90}. These constant differences between each pair of alloys can be readily seen in Fig. 6.

Because eqn (2) with the simplified parameters in Table 3(b) can describe deformation in each base alloy and its Cr-modification, plastic flow in the Cr-bearing materials is almost entirely dictated by the NiAl-AlN matrices. Hence the current ~10 vol % Cr additions have little effect on the controlling creep mechanism(s). The relative weakness of pure Cr at elevated temperature can be seen in Fig. 7 which illustrates its expected strength between 1200 and 1400 K (dashed lines). These predictions are based on a

temperature compensated power law fit of Stephens and Kloop's creep data [32] for 230 and 90 μm grain size polycrystalline Cr tested at 1089, 1255 and 1422 K, where

$$\dot{\varepsilon} = 25.5\,\sigma^{5.44}\exp(-353.1/(RT)), \tag{5}$$

with $R_d^2 = 0.912$ and the standard deviations of the stress exponent and activation energy being 0.28 and 19.6 kJ/mol, respectively. Contrasting the predicted behavior of pure Cr (Fig.7) to that of the base NiAl-AlN alloys (Figs 5(a,c,e)) strongly implies that Cr additions would impair elevated temperature strength: for example a stress of ~10 MPa should produce a creep rate of 10^{-7} s^{-1} in Cr at 1300 K while stresses ranging from 70 to 100 MPa would be required for the current three NiAl-AlN materials.

Since both the NiAl-AlN matrix and Cr flakes can plastically deform between 1200 and 1400 K, the most logical deformation model is a constant strain rate approach, where the applied load is redistributed between each phase until both creep at the same rate. Thus the strength of the composite σ_C at a constant strain rate is given by a Rule of Mixtures, or

$$\sigma_C = \sigma_M V_M + \sigma_{Cr} V_{Cr} \tag{6}$$

where σ_M & σ_{Cr} are the stresses required to produce the same constant strain rate in the NiAl-AlN matrix & pure Cr and V_M & V_{cr} are the volume fractions of matrix and Cr. By rearrangement of the terms in eqn (6) and use of the relationship that $V_M + V_{Cr} = 1$, the stress on the NiAl-AlN portion of each composite is

$$\sigma_M = (\sigma_C - \sigma_{Cr} V_{Cr})/(1-V_{Cr}). \tag{7}$$

Eqn (7) can then be evaluated for every set of composite strength and strain rate data, where eqn (5) and the composite strain rate values are used to determine the appropriate σ_{Cr}'s for use in each calculation along with the volume fraction of Cr reported in Table 1.

Use of eqns (5 and 7) to predict the stress on the NiAl-AlN matrix for alloy 90 (Ni-49.5Al-11.4AlN+11.1Cr) is illustrated in Table 4. Because of the relative weakness of Cr, the redistribution of load increases the stress on the NiAl-AlN matrix over that experienced by the composite as a whole. If these σ_M values are realistic, they then should predict the same creep rate in the unmodified matrix (alloy 91) as was measured in the Cr-containing composite. The predicted creep rates due to the Rule-of-Mixtures σ_M values are also given in Table 4 and illustrated as a function of the measured composite creep rates in Fig. 8, where there appears to be a one-to-one correspondence between prediction and measurement over 5 orders of magnitude in strain rate and three distinct test temperatures. This goodness of fit was confirmed by linear regression analysis, where the regression line in Fig. 8. has a slope of 1.00 with a coefficient of deviation of 0.982. Repetition of the analysis for the other two pairs of alloys (87/86 and L24/L25) yielded similar results, where the regression fits between creep rate due to the Rule-of-Mixtures σ_M values as a function of the measured composite creep rate gave slopes of 1.03 ($R_d^2 = 0.992$) for 87/86 and 0.93 ($R_d^2 = 0.949$) for L24/L25.

In summary, the creep behavior in the present NiAl-AlN +Cr composites can be understood through the simple Rule-of-Mixtures model, where load is shed from the weak phase to the strong phase in order to maintain an equal strain rate in each constituent. Due to the weakness of Cr in comparison to the NiAl-AlN matrix and the relatively low volume fraction of Cr, deformation is completely dominated by the strong matrix. Since the properties of our composites can be completely traced to those of the unmodified NiAl-AlN matrices, this implies that Cr is an ineffective solid solution/precipitation strengthening agent between 1200 and 1400 K.

The inability of the Cr flakes to provide some increase in creep strength was not expected as prior work on directionally solidified NiAl-Cr eutectics had demonstrated significant improvements: for example directionally solidified NiAl-34Cr requires a stress of ~ 100 MPa to produce a strain rate of 10^{-7} s^{-1} at 1300 K while a [100] NiAl single crystal would require a stress of 10 MPa [31]. While directionally

solidified NiAl-34Cr does contain about three and a half times more Cr than the current composites, an increased amount of a weak component would not strengthen. Since both NiAl [4] and Cr [32] are weak, we believe that strength of directionally solidified NiAl-34Cr must derive from the reduced dimensions ($\leq$ 1 μm) of the fibers/lamella which limit the size of subgrains formed during deformation. Subgrains are formed during creep of both Cr [32] and NiAl [4] and strength is inversely dependent on the subgrain size [33]; therefore thin Cr and/or NiAl fibers/lamella should be strong.

Based on the current findings, it should be possible to design a hot extruded cryomilled NiAl + Cr composite with optimized creep and toughness properties. With elevated temperature strength of cryomilled NiAl being proportional to the square root of the AlN content [30], improvements in creep resistance can be made through the use of higher AlN content matrices. On the other hand significant increases in the room temperature fracture toughness will probably require more than the present 10 vol % Cr which would, of course, tend to reduce the elevated temperature strength by reducing the matrix volume fraction. The unknown factor is the role of hot extrusion on behavior. While densification by hot extrusion is necessary to improve the toughness over that of the matrix, the influence of extrusion temperature and/or reduction ratio on the properties of cryomilled NiAl + Cr are not known. Once the effects of extrusion parameters on toughness have been determined, it should be possible to develop an alloy composition (AlN and Cr content) and extrusion parameters for optimium mechanical properties

SUMMARY OF RESULTS

Cryomilled NiAl powder containing two levels of AlN has been blended with Cr flakes in an effort to improve the room temperature toughness without severely affecting the elevated temperature strength. Although, little improvement in toughness was measured in NiAl-AlN+10 vol % Cr composites which were consolidated by hot isostatic pressing, the toughness of hot extruded NiAl-6.5AlN + 10.5Cr was more than twice that determined for the base NiAl-AlN alloy. The elevated temperature plastic flow

properties of the Cr-modified composites were completely controlled by the NiAl-AlN matrices. This behavior could be successfully described with a Rule-of-Mixtures model, where load was shed from the weak Cr to the strong matrix.

Table 1. Consolidation Techniques and Compositions of Cryomilled NiAl-based Materials

Identification	Matrix Composition[1] At. %	Second Phase Content, Vol. %			Densification Procedure
	Al	AlN	Cr	Al_2O_3	
87	50.3	7.4	0	1.3	HIP @ 1495 K-138 MPa- 6 h
86	50.	6.5	10.2	1.3	HIP @ 1495 K-138 MPa- 6 h
L24	51	7.3	0	1.1	Hot Extruded @ 1505 K - 8:1
L25	51.1	6.5	10.5	0.9	Hot Extruded @ 1505 K - 8:1
91	49.8	12.4	0	1.1	HIP @ 1495 K-138 MPa- 6 h
90	49.5	11.4	11.1	1.2	HIP @ 1495 K-138 MPa- 6 h

[1] Small amounts (<0.1 wt. %) of C, Cu, Fe, Mo, and Si were also generally found.

Table 2. Room Temperature Mechanical properties of Cryomilled NiAl-based Materials

Identification	Elastic Modulus, Gpa			Yield Strength, MPa	Fracture Strength, MPa	Toughness, Average MPa√m	Stan. Dev.
	Dynamic	Bend	Predicted[1]				
87	202	188	197	344	666	4.6	0.4
86	205	187	202	162	184	6.2	0.7
L24	193	179	-	232	529	-	-
L25	176	175	-	193	389	11.2	2.3
91	203	186	204	227	617	-	-
90	210	199	209	147	193	7.7	0.7

[1] Prediction based on Rule of Mixtures

Table 3. Temperature compensated exponential law descriptions of the flow stress - strain rate - temperature behavior for cryomilled NiAl-based alloys

Identification	A, s^{-1}	C	δ_C	Q, kJ/mol	δ_Q,	R_d^2
			(a) Individual Fits			
87	5.34×10^9	0.0792	0.0027	-490.5	19.4	0.995
86	3.73×10^9	0.0801	0.0022	-476.3	16.9	0.994
L24	5.26×10^8	0.0573	0.0028	-457.9	41.7	0.973
L25	7.01×10^{10}	0.0638	0.0035	-502.3	48.4	0.955
91	1.21×10^{12}	0.0569	0.0024	-543.4	32.3	0.973
90	4.88×10^{11}	0.0605	0.0024	-515.0	30.3	0.985
			(b) Combined Fits			
87	1.88×10^9	0.0805	0.0017	-481.4	12.5	0.994
86	6.40×10^9					
L24	1.45×10^9	0.0605	0.0023	-474.7	33.1	0.959
L25	8.79×10^9					
91	3.36×10^{11}	0.0581	0.0018	-531.8	23.7	0.975
90	3.28×10^{12}					

Table 4. Rule of Mixture calculation of the stress on the NiAl-AlN matrix in a Ni-49.5Al-11.4AlN +11.1Cr composite and the predicted deformation rate in the unmodified base Ni-49.8Al-12.4AlN alloy.

Composite Test Parameters			Stress on Pure Cr in Composite	Stress on Matrix in Composite	Predicted Strain Rate in Unmodified Matrix[1]
Temp, K	Stress, MPa	Strain Rate, s^{-1}	(σ_{Cr}), MPa	(σ_M), MPa	($\dot{\varepsilon}_{91}$), s^{-1}
1200	269	3.27×10^{-4}	84.6	292	1.09×10^{-4}
1200	223.1	2.32×10^{-5}	52	244.5	7.29×10^{-6}
1200	187.9	1.79×10^{-6}	32.5	207.3	8.80×10^{-7}
1200	159.3	1.66×10^{-7}	21	176.6	1.53×10^{-7}
1300	210.1	2.17×10^{-4}	47.5	230.4	2.02×10^{-4}
1300	176.9	2.22×10^{-5}	31.3	195.1	2.70×10^{-5}
1300	121.5	1.95×10^{-6}	20.	134.2	8.44×10^{-7}
1300	81.2	1.84×10^{-7}	13.	89.7	6.73×10^{-8}
1300	71.4	5.78×10^{-8}	10.5	79.	3.66×10^{-8}
1300	49.6	1.60×10^{-8}	8.3	54.8	9.21×10^{-9}
1400	144.3	1.85×10^{-4}	30.	158.6	1.16×10^{-4}
1400	109	2.19×10^{-5}	20.3	120.1	1.29×10^{-5}
1400	49.3	1.03×10^{-6}	11.6	54.	3.01×10^{-7}

[1] From Table 3(a), where $\dot{\varepsilon}_{91} = 1.21 \times 10^{12} \exp(0.0596\sigma_M)\exp(-543.4/RT)$

REFERENCES

1. C.T. Liu and K.S. Kumar, *JOM* **45**(5) (1993) 38-44.
2. D.B. Miracle, *Acta Metall. Mater.* **41** (1993) 649-84.
3. R.D. Noebe, R.R. Bowman and M.V. Nathal, *Inter. Mater. Rev.* **38** (1993) 193-232.
4. J.D. Whittenberger. *J. Mat. Sci.* **22** (1987) 394-402.
5. K.R. Forbes, U. Glatzel, R. Darolia and W.D.Nix, *Met. Mat. Trans. A* **27A** (1996) 1229-40.
6. J.D Whittenberger, I.E. Locci, Ram Darolia and R. Bowman. *Mater.Sci. Eng. A.* **A268** (1999) 165-83.
7. J.D. Whittenberger , Michael V. Nathal and Patrica O. Book. *Scripta Metall. et Mater.* **28** (1993) 53-8
8. R. Noebe and W.S. Walston, Structural Intermetallics 1997 (eds. M.V. Nathal, R. Darolia, C.T. Liu, P.L. Martin, D.B. Miracle, R. Wagner and M. Yamaguchi) TMS, Warrendale, PA, 1997, pp. 573-84.
9. R. Darolia and W.S. Walston, Structural Intermetallics 1997 (eds. M.V. Nathal, R. Darolia, C.T. Liu, P.L. Martin, D.B. Mircle, R. Wagner and M. Yamaguchi) TMS, Warrendale, PA, 1997, pp. 585-94.
10. J.D Whittenberger , I.E. Locci, Ram Darolia and R. Bowman, *Mater.Sci. Eng. A.* **A268** (1999) 165-83.
11. E. Arzt and P. Grahle, High-Temperature Ordered Intermetallic Alloys VI, Vol. **364**, Part 1; (eds. J.A. Horton, I. Baker, S. Hanada, R.D. Noebe and D.S. Schwartz), Materials Research Society, Pittsburgh, PA, 1995, pp. 525-36.
12. E. Arzt and P. Grahle, Acta Mater. **46** (1998) 2717-2727.
13. H. Choo, P. Nash and M. Dollar, *Mater. Sc. Eng. A* **239-240** (1997) 464-471
14. J.D. Whittenberger, Structural Intermetallics, (eds. R. Darolia, J.J. Lewandowski, C.T. Liu, P.L. Martin, D.B. Miracle and M.V. Nathal) TMS, Warrendale, PA 1993, pp. 819-28.
15. D.R. Johnson, X.F. Chen, B.F. Oliver, R.D Noebe and J.D. Whittenberger. *Intermetallics* **3** (1995) 99-113.
16. J.D. Cotton, R.D. Noebe and M.J. Kaufman, Structural Intermetallics, (eds. R. Darolia, J.J. Lewandowski, C.T. Liu, P.L. Martin, D.B. Miracle and M.V. Nathal) TMS, Warrendale, PA 1993, pp. 513-22.
17. B. Schietinger, Fortschritt-Berichte, VDI Reihe 5 Nr. 410. Düsseldorf, Germany, 1995.
18. S.M. Lane, S.B. Biner and O. Buck, Mater. Sci. Eng. **A246** (1998) 244-51.
19. B.J.M. Aikin, J.D. Whittenberger and M.G. Hebsur. Mechanical Alloying for Structural Applications, (eds. J.J. deBarbadillo, F.H. Froes and R. Schwarz), ASM International, Materials Park, OH, 1993, pp. 283-90.
20. "Standard Test Method for determination of Fracture Toughness of Advanced Ceramics at Ambient Temperature," Test Method C1421-99, American Society for Testing Materials Annual Book of Standards, 15.01 ASTM, West Conshohocken, PA, 2000.
21. ASTM C 1259-94, "Standard Test Method for Dynamic Young's Modulus, Shear Modulus, and Poisson's Ratio for Advanced Ceramics by Impulse Excitation of Vibration," American Society for Testing and Materials Annual Book of Standards, Vol. 15.01, pp. 336-384, 1995.
22. J.A. Salem, L.J. Ghosn, and M.G. Jenkins, Ceramic Engineering and Science Proceedings, 19 (1998) 587-594.
23. M.R.Harmouche and A. Wolfenden, *J. Testing Evaluation* **15** (1987) 101-104.
24. J. L. Walter and H. E. Cline, *Metall. Trans.*, **1** (1970) 1221-1229.
25. W.H. Tian, C.S. Han, M. Nemoto, *Intermetallics* **7** (1999) 59-67.
26. R.D. Noebe, R.R. Bowman and M.V. Nathal, Physical Metallurgy and Processing of Intermetallic Compounds, eds. N.S. Stoloff and V.K. Sikka, Chapman and Hall, New York, NY, USA, 1996, pp. 212-296.
27. D. Gerlick, S.L. Dole and G.A. Slack, *J.Phys. Chem. Solids* **47** (1986) 437-441.
28. P.E. Armstrong and H.L. Brown, *Trans. AIME* **230** (1964) 962-66.

29. A. Wolfenden, C.M. Miller and M.G. Hebsur, J. Mater. Sci. Lett. **17** (1998) 1861-64.
30. M.H. Hebsur, J.D. Whittenberger and A. Garg, Structural Intermetallics 1997 (eds. M.V. Nathal, R. Darolia, C.T. Liu, P.L. Martin, D.B. Mircle, R. Wagner and M. Yamaguchi) TMS, Warrendale, PA, 1997, pp. 621-30.
31. D.R. Johnson, X.F. Chen, B.F. Oliver, R.D. Noebe and J.D. Whittenberger, *Intermetallics* **3** (1995) 99-113.
32. J.R. Stephens and W.D. Kloop, *J. Less Com Metals* **27** (1972) 87-94.
33. S. V. Raj and G. M. Phaar, *Mater. Sci. Eng.* **81** (1986) 217-37.

FIGURE CAPTIONS

1. Unetched light optical photomicrographs of as-extruded Ni-51.1Al + 6.5AlN + 10.5 vol. % Cr {Alloy L25, Table 1}. (a,c) are transverse sections and (b,d) are longitudinal sections

2. Unetched light optical photomicrographs of HIP'ed Cr-modified cryomilled NiAl. (a,b) Ni-49.5Al + 11.4AlN + 11.1 vol. % Cr {Alloy 90, Table 1} and (c,d) Ni-50.Al + 6.5AlN + 10.2 vol. % Cr {Alloy 86, Table 1}.

3. True 1300 K compressive stress - strain curves for HIP'ed (a) Ni-49.8Al+12.4AlN and (b) Ni-49.5Al + 11.4AlN + 11.1 vol. % Cr as a function of nominal strain rate

4. True 1300 K compressive creep curves for cryomilled NiAl with and without Cr additions as a function of engineering stress. (a) HIP'ed NiAl + ~12AlN and (b) hot extruded NiAl + ~7AlN.

5. True compressive flow stress - strain rate - temperature behavior of (a) HIP'ed Ni-51Al+7.3AlN, (b) HIP'ed Ni-51.1Al+6.5AlN+10.5Cr, (c) hot extruded Ni-50.3Al+7.4AlN, (d) hot extruded Ni-50Al+6.5AlN+10.2Cr, (e) HIP'ed Ni-49.8Al+12.4AlN, and (f) HIP'ed Ni-49.5Al+11.4AlN+11.1Cr. Open symbols represent results from constant velocity testing; filled symbols represent results from constant load creep testing.

6. Combined true compressive flow stress - strain rate - temperature behavior for each pair of base and Cr-modified alloys. (a) Alloys 87 and 86, (b) Alloys L24 and L25 and (c) Alloys 91 and 90. Solid lines and symbols describe the base alloys, while the dashed lines and open symbols describe the Cr-modified alloys.

7. Predicted creep properties of Cr as estimated from elevated temperature testing of 230 and 90 μm grain sized polycrystalline, high purity Cr [32].

8. Rule-of-Mixtures predicted creep rate for the cryomilled NiAl matrix in alloy 90 {alloy 91} as a function of the experimentally measured creep rate for the composite {alloy 90}.

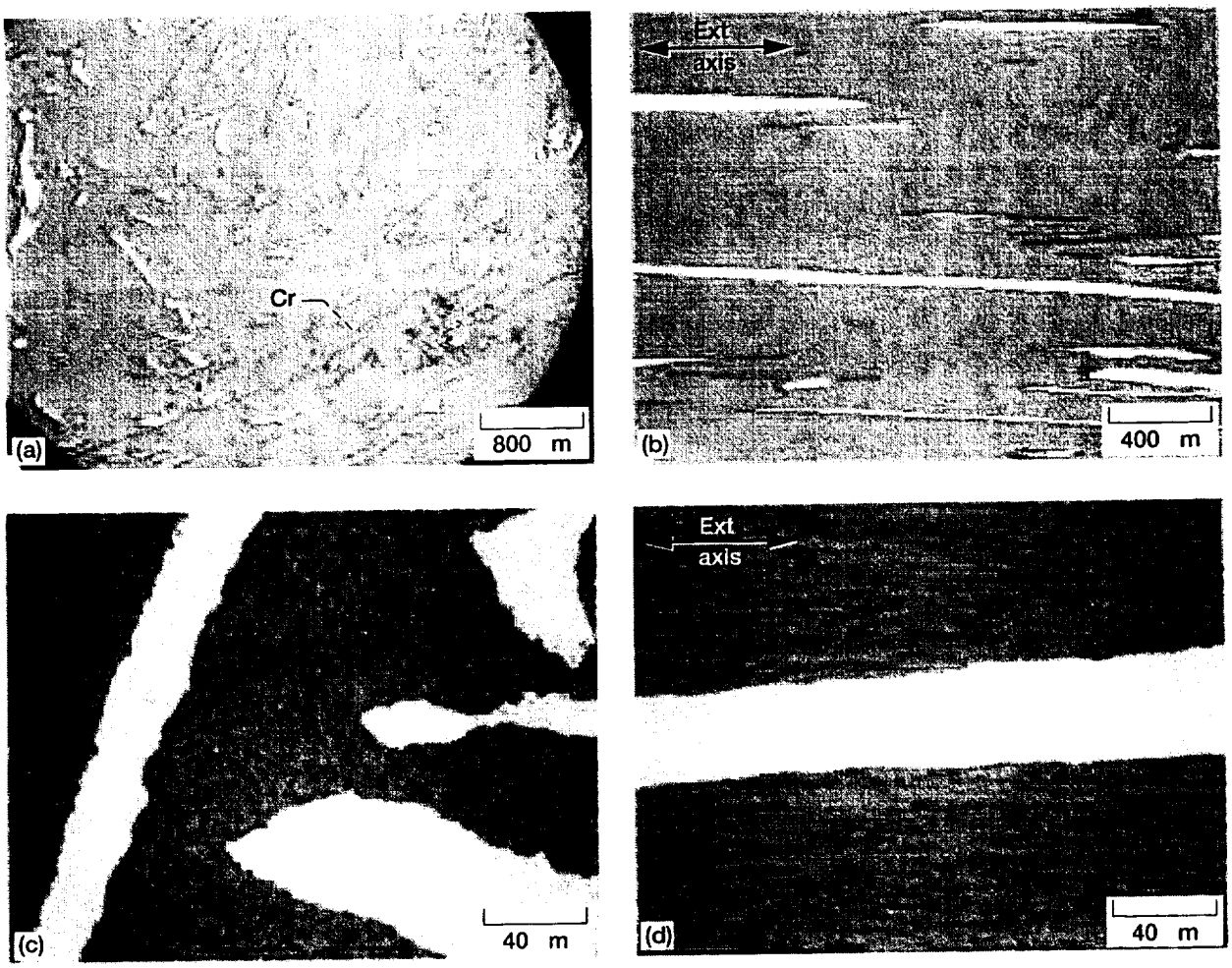

Fig 1

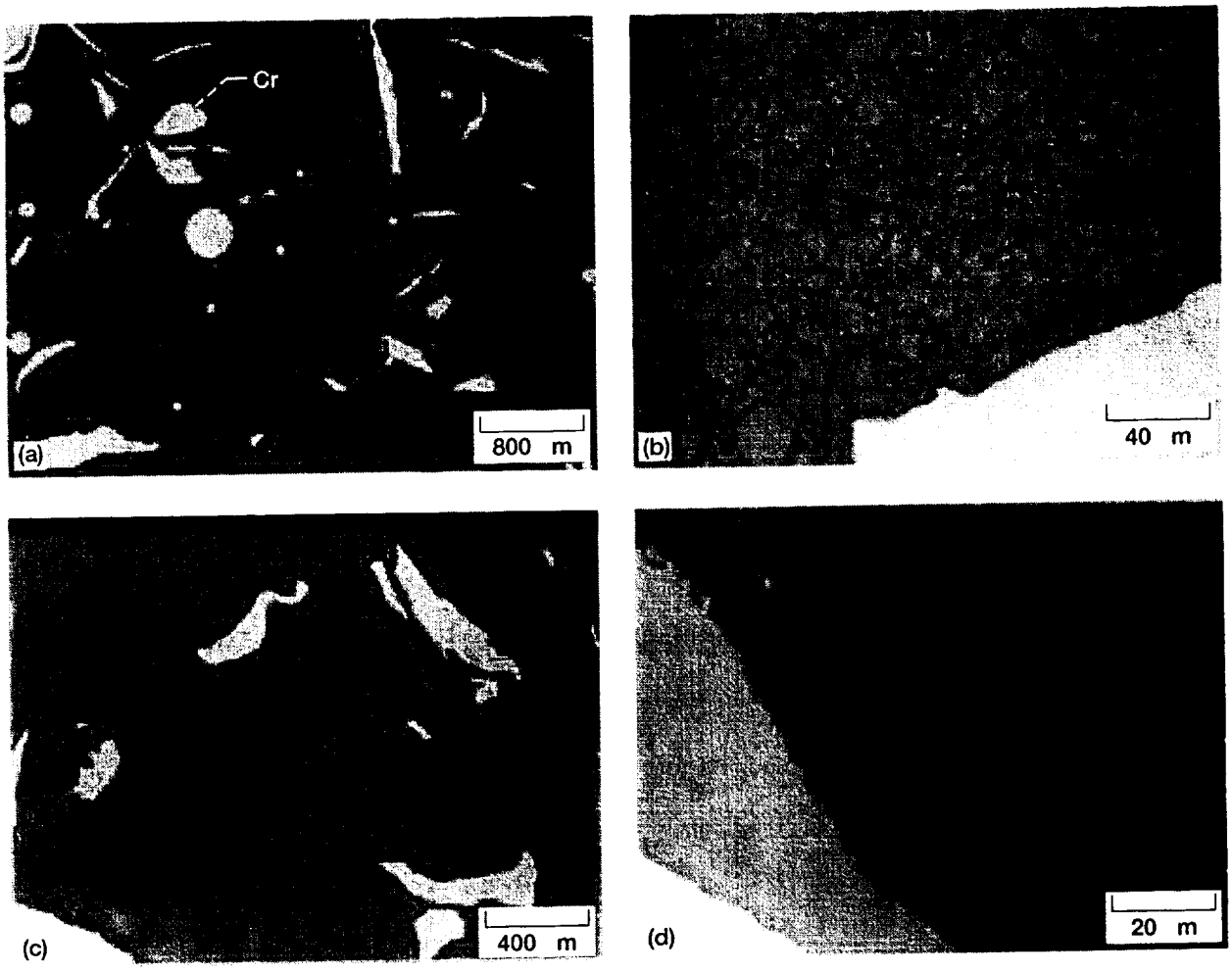

Fig 2

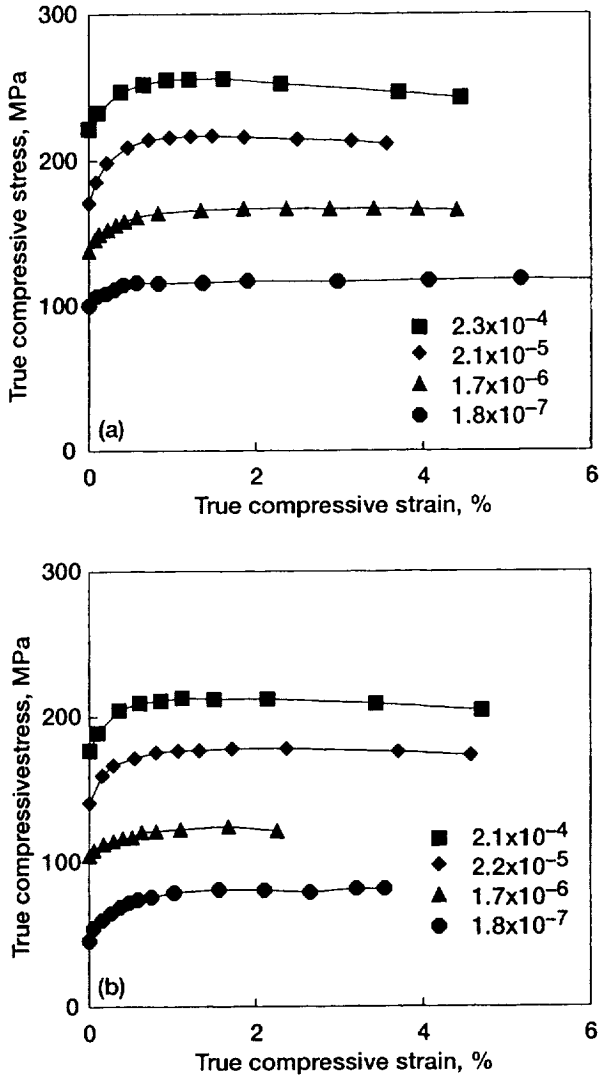
300
200
100
0
True compressive stress, MPa
2.3x10^{-4}
2.1x10^{-5}
1.7x10^{-6}
1.8x10^{-7}
(a)
0
2
4
6
True compressive strain, %
300
200
100
0
True compressivestress, MPa
2.1x10^{-4}
2.2x10^{-5}
1.7x10^{-6}
1.8x10^{-7}
(b)
0
2
4
6
True compressive strain, %

Fig 3

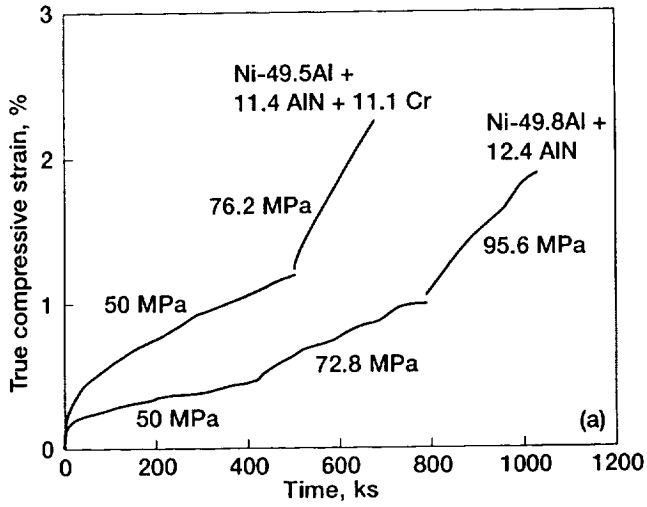
Ni-49.5Al +
11.4 AlN + 11.1 Cr
Ni-49.8Al +
12.4 AlN
76.2 MPa
95.6 MPa
50 MPa
72.8 MPa
50 MPa
(a)
True compressive strain, %
Time, ks
0
1
2
3
0
200
400
600
800
1000
1200

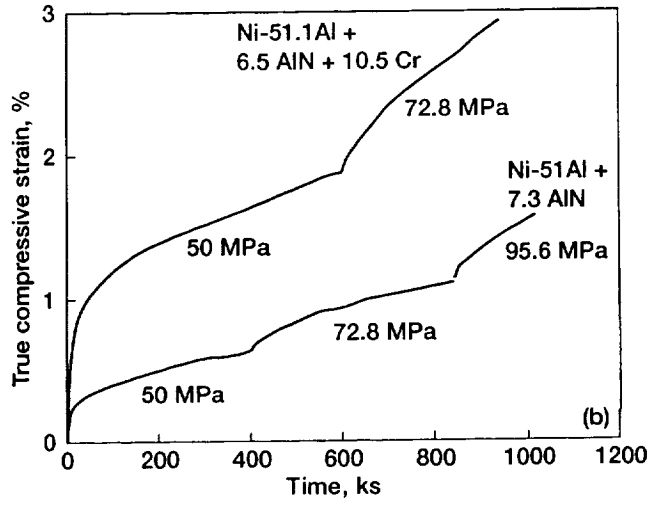
Ni-51.1Al +
6.5 AlN + 10.5 Cr
72.8 MPa
Ni-51Al +
7.3 AlN
50 MPa
95.6 MPa
72.8 MPa
50 MPa
(b)
True compressive strain, %
Time, ks
0
1
2
3
0
200
400
600
800
1000
1200

Fig 4

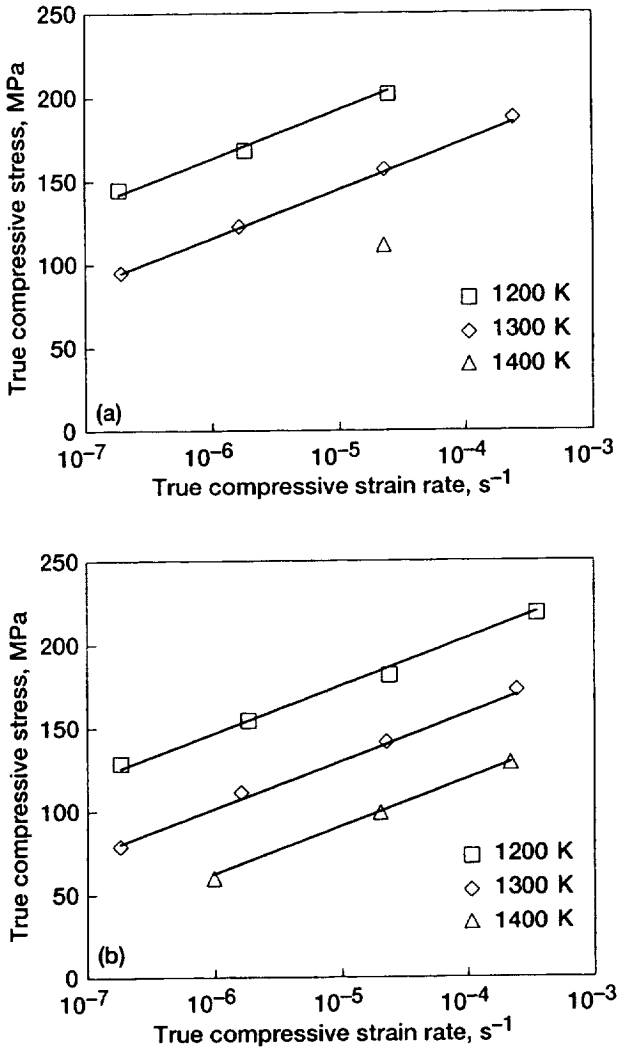
250
200
150
100
50
0
True compressive stress, MPa
1200 K
1300 K
1400 K
(a)
10^{-7}
10^{-6}
10^{-5}
10^{-4}
10^{-3}
True compressive strain rate, s^{-1}
250
200
150
100
50
0
True compressive stress, MPa
1200 K
1300 K
1400 K
(b)
10^{-7}
10^{-6}
10^{-5}
10^{-4}
10^{-3}
True compressive strain rate, s^{-1}

Fig 5

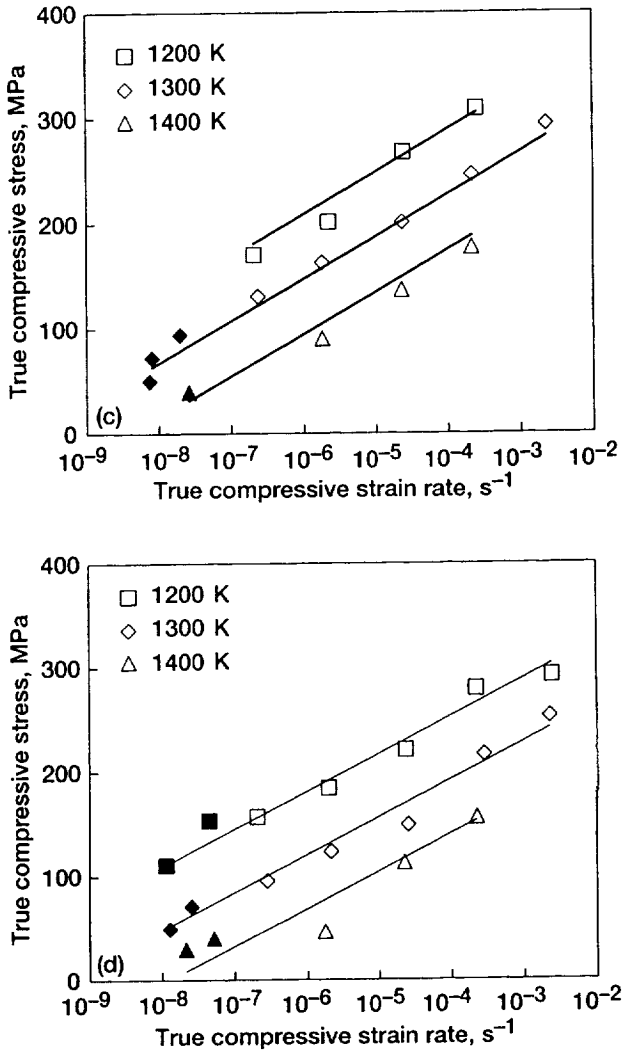
400
300
200
100
0
True compressive stress, MPa
1200 K
1300 K
1400 K
(c)
10^{-9} 10^{-8} 10^{-7} 10^{-6} 10^{-5} 10^{-4} 10^{-3} 10^{-2}
True compressive strain rate, s^{-1}
400
300
200
100
0
True compressive stress, MPa
1200 K
1300 K
1400 K
(d)
10^{-9} 10^{-8} 10^{-7} 10^{-6} 10^{-5} 10^{-4} 10^{-3} 10^{-2}
True compressive strain rate, s^{-1}

Fig 5

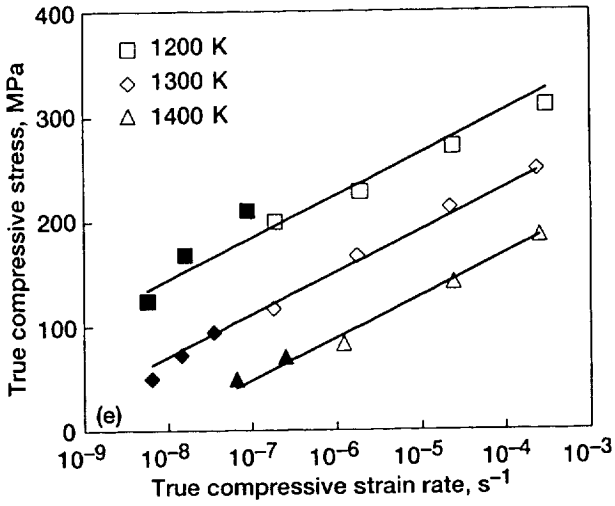
400
300
200
100
0
True compressive stress, MPa
□ 1200 K
◇ 1300 K
△ 1400 K
(e)
10^{-9} 10^{-8} 10^{-7} 10^{-6} 10^{-5} 10^{-4} 10^{-3}
True compressive strain rate, s^{-1}

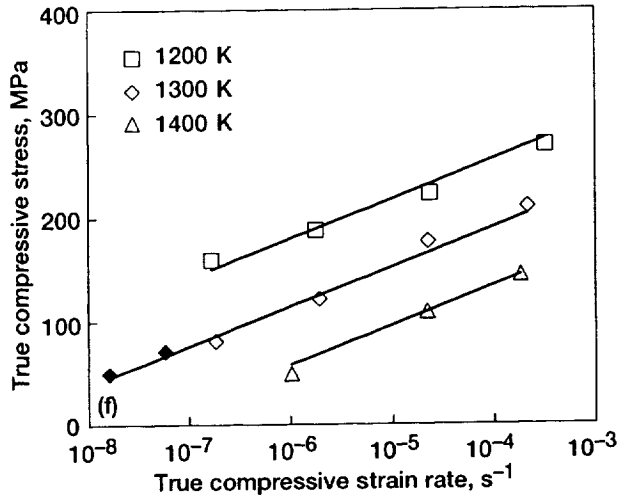
400
300
200
100
0
True compressive stress, MPa
□ 1200 K
◇ 1300 K
△ 1400 K
(f)
10^{-8} 10^{-7} 10^{-6} 10^{-5} 10^{-4} 10^{-3}
True compressive strain rate, s^{-1}

Fig 5

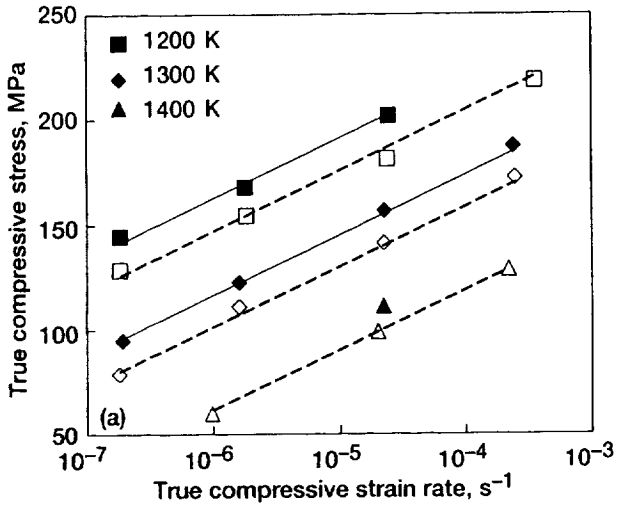
250
200
150
100
50
True compressive stress, MPa
1200 K
1300 K
1400 K
(a)
10^{-7}
10^{-6}
10^{-5}
10^{-4}
10^{-3}
True compressive strain rate, s^{-1}

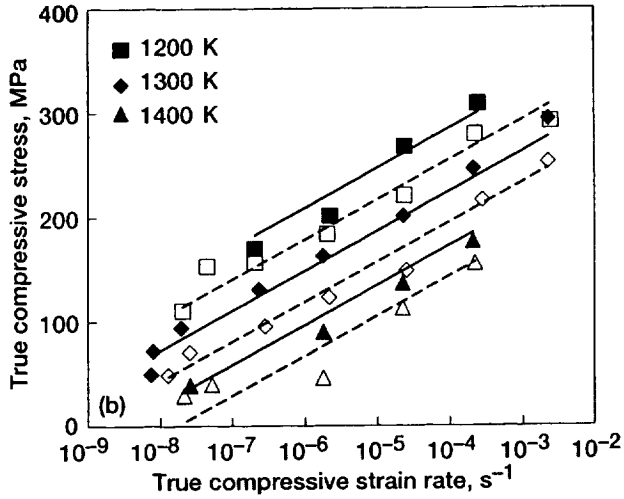
400
300
200
100
0
True compressive stress, MPa
1200 K
1300 K
1400 K
(b)
10^{-9}
10^{-8}
10^{-7}
10^{-6}
10^{-5}
10^{-4}
10^{-3}
10^{-2}
True compressive strain rate, s^{-1}

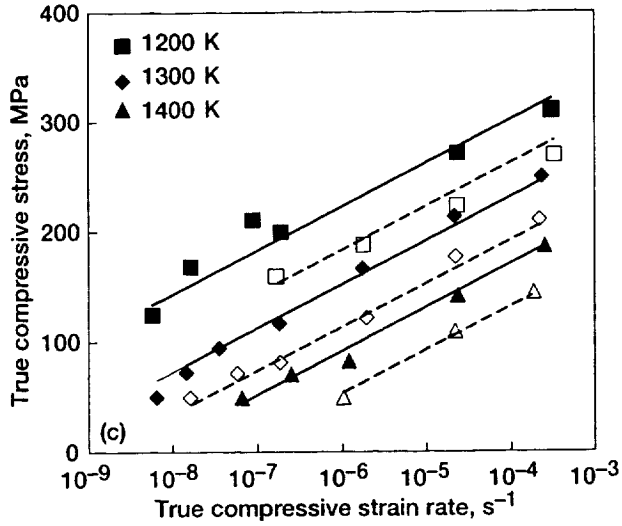
400
300
200
100
0
True compressive stress, MPa
1200 K
1300 K
1400 K
(c)
10^{-9}
10^{-8}
10^{-7}
10^{-6}
10^{-5}
10^{-4}
10^{-3}
True compressive strain rate, s^{-1}

Fig 6

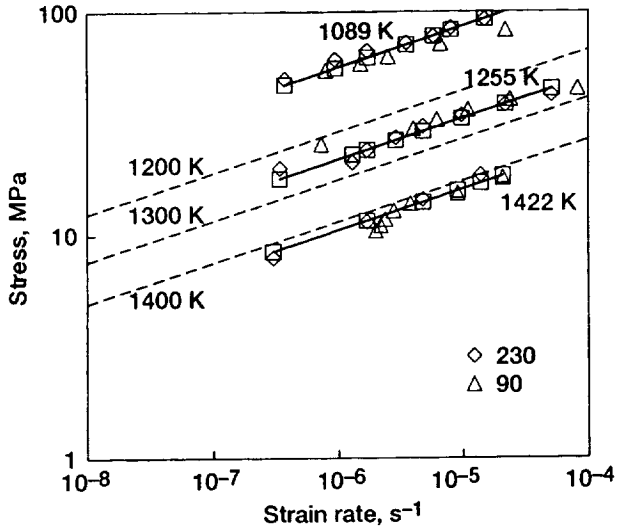
100
10
1
Stress, MPa
1089 K
1255 K
1422 K
1200 K
1300 K
1400 K
◇ 230
△ 90
10⁻⁸
10⁻⁷
10⁻⁶
10⁻⁵
10⁻⁴
Strain rate, s⁻¹

Fig 7

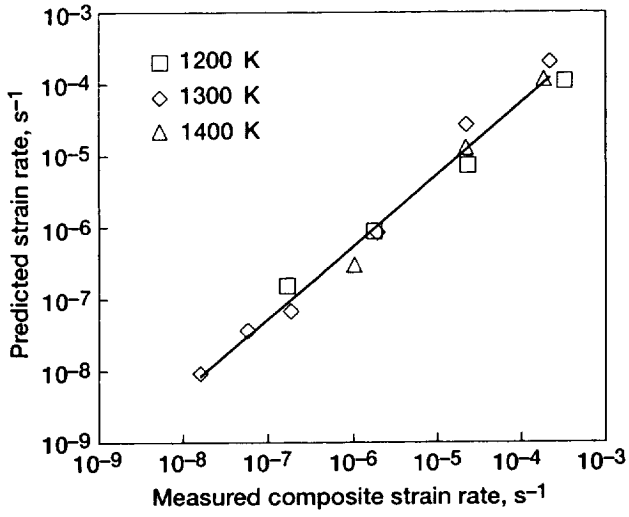
□ 1200 K
◇ 1300 K
△ 1400 K
Predicted strain rate, s⁻¹
Measured composite strain rate, s⁻¹
10⁻³
10⁻⁴
10⁻⁵
10⁻⁶
10⁻⁷
10⁻⁸
10⁻⁹

Fig 8